International Journal of Minerals, Metallurgy and Materials
Volume 24, Number 5, May 2017, Page 493
DOI: 10.1007/s12613-017-1430-5

Reduction behavior and kinetics of vanadium–titanium sinters under high potential oxygen enriched pulverized coal injection

Jin-fang Ma[1)], *Guang-wei Wang*[1)], *Jian-liang Zhang*[1)], *Xin-yu Li*[2)], *Zheng-jian Liu*[1)], *Ke-xin Jiao*[1)], *and Jian Guo*[1)]

1) School of Metallurgical and Ecological Engineering, University of Science and Technology Beijing, Beijing 100083, China
2) Plans and Operations Department, Wanbao Mining Ltd., Beijing 100053, China
(Received: 19 August 2016; revised: 23 December 2016; accepted: 26 December 2016)

Abstract: In this work, the reduction behavior of vanadium–titanium sinters was studied under five different sets of conditions of pulverized coal injection with oxygen enrichment. The modified random pore model was established to analyze the reduction kinetics. The results show that the reduction rate of sinters was accelerated by an increase of CO and H_2 contents. Meanwhile, with the increase in CO and H_2 contents, the increasing range of the medium reduction index (MRE) of sinters decreased. The increasing oxygen enrichment ratio played a diminishing role in improving the reduction behavior of the sinters. The reducing process kinetic parameters were solved using the modified random role model. The results indicated that, with increasing oxygen enrichment, the contents of CO and H_2 in the reducing gas increased. The reduction activation energy of the sinters decreased to between 20.4 and 23.2 kJ/mol.

Keywords: ore reduction; sintering; oxygen enrichment; pulverized coal; injection; kinetic models

1. Introduction

Currently, China's iron and steel industry is in a rigid condition known as the "new normal." One key objective of iron and steel plants is to reduce costs and increase profits while ensuring sufficient product quality. At present, research into the raw and fuel materials used in blast furnaces is focused primarily on the sinter ores and coke. With respect to sinter, as the iron ore process environment becomes increasingly complex, various iron ores are being used in the sinter blending process [1–4]; among these sinters, vanadium–titanium sinter has been studied broadly because of its special characteristics. Previous studies on sinters have concentrated on their mineral components, structure, reducibility, strength, and furnace protection characteristics. Deng [5] studied the reduction process of vanadium–titanium sinter and the slag-iron formation process in a blast furnace by observing the anatomy in a 0.8-m^3 blast furnace. Liu *et al*. [6] found that the controlling step in the solid-state reduction of pre-oxidized vanadium–titanium magnetite concentrate is the interface chemical reaction when coal is used as the reducing agent, indicating that vanadium–titanium magnetite concentrate is difficult to reduce. Bai *et al*. [7] studied the mineralogical phase of vanadium–titanium sinters during the reduction degradation process. Other researchers have focused on the influence of ω(MgO) on the strength of vanadium–titanium sinters and on the sintering process [8–10]. Yang *et al*. [11] investigated the influence of various addition ratios of vanadium–titanium magnetite concentrate on the metallurgical properties of vanadium–titanium sinter. Sun *et al*. [12] studied the furnace protection role of titanium-containing sinters in blast furnaces. With respect to coke, numerous studies on substituting coal for coke to reduce the coke ratio and strengthen the blast furnace smelting performance have been reported; hence, oxygen-enrichment pulverized coal injection in blast furnaces has emerged as an active research topic.

Some recent studies have focused on the changing conditions in blast furnaces after oxygen-enrichment pulve-

Corresponding author: Guang-wei Wang E-mail: wgw676@163.com

rized-coal injection. Zhu and Wang [13] reported that iron-ore reduction in a blast furnace was improved after oxygen-enrichment pulverized coal injection. Babich *et al*. [14] noted the difficulty of pulverized coal injection and indicated the possibility of increasing the pulverized coal combustion ratio from both theoretical and practical viewpoints. Ghanbari *et al*. [15] discussed the influence of using pulverized coal and also proposed restricted conditions. Shen *et al*. [16] used a model to investigate the influence of pulverized coal characteristics and blast furnace conditions on the pulverized coal injection process. Yan *et al*. [17] analyzed the influence of high oxygen enrichment pulverized coal injection on the tuyeres, gas, and smelting cost of blast furnaces. Hao *et al*. [18] investigated the influence of the metallization degree of burden on the oxygen enrichment pulverized coal injection in the blast furnace smelting process and obtained the corresponding complementary relationship between the two sides. However, the literature lacks information concerning the sinter reduction kinetics in the case of high reduction potential conditions. Kinetics analysis is also necessary for the design and operation of ironmaking systems, which is essential for further studies in this field.

In summary, extensive works related to vanadium–titanium sinters and oxygen enrichment pulverized coal injection have been reported; however, their mutual effect has not been investigated. In fact, the relationship between them should be elucidated because they are used in blast furnaces simultaneously, influencing the whole production process and, in some cases, having complementary effects. The goal of the present work is to investigate the isothermal reduction behaviors of vanadium–titanium sinters under various high potential pulverized coal injection conditions. The kinetic parameters were also calculated using established kinetic models. Hence, the results of this paper are expected to provide theoretical support and reference data for further studies of vanadium–titanium magnetite.

2. Experimental and methods

In this work, the vanadium–titanium sinters were provided by Panzhihua Iron and Steel Company of China. The size of the sinters used in the reduction experiments was 10–12.5 mm; their chemical composition is shown in Table 1. As shown in Table 1, the TFe of the sinters was only 48.7wt%, and the CaO and SiO_2 contents were higher than those of normal sinters produced using other iron ores. The TiO_2 and V_2O_5 contents were as high as 5.20wt% and 0.34wt%, respectively. The reduction of these sinters would likely consume a relatively high volume of reducing gas and produce a large amount of slag after reduction, adversely affecting normal operation of the blast furnace.

Table 1. Chemical composition of vanadium–titanium sinters

wt%

TFe	FeO	CaO	SiO_2	MgO	Al_2O_3	MnO	V_2O_5	TiO_2
48.70	9.06	12.5	6.63	2.08	5.29	0.35	0.34	5.20

The isothermal reduction experiments were conducted using five different reducing atmospheres. In each batch, approximately 30 g of sinter was used. The experimental temperature was increased from room temperature to the reaction temperature at a rate of 10°C/min, and the sinters were protected under an atmosphere of purified N_2. Five different reducing atmospheres were designed as follows. Condition 1 (C1) represents the total coke smelting cycle, which is the basic cycle shown in Table 2; condition 2 (C2) represents the high potential pulverized coal injection with non-oxygen enrichment; condition 3 (C3), condition 4 (C4), and condition 5 (C5) represent the high potential pulverized coal injection with oxygen enrichments of 9vol%, 19vol%, and 39vol%, respectively. The gas composition was calculated based on previous research [19]. Because indirect reduction strongly influences the economic and technical indexes of the blast furnace, the quick indirect reduction temperature zone was used as the isothermal reduction temperature in this research; the investigated temperatures were 800, 900, 1000, 1100, and 1200°C, respectively. The flow of the reducing gas was 10 L/min to eliminate the influence of external diffusion on the reduction process.

Table 2. Reduction conditions of vanadium–titanium sinters

Blast furnace operation	Working condition	Reaction temperature / °C	Gas flow / ($L \cdot min^{-1}$)	Gas composition / vol%		
				CO	N_2	H_2
Basic period	C1	800–1200	10	45.0	55.0	0
Non-oxygen enrichment	C2	800–1200	10	45.0	50.0	5.0
9vol% oxygen enrichment	C3	800–1200	10	50.0	42.5	7.5
19vol% oxygen enrichment	C4	800–1200	10	60.0	30.0	10.0
39vol% oxygen enrichment	C5	800–1200	10	70.0	12.5	17.5

The vanadium–titanium sinters were reduced in a thermogravimetric analysis apparatus as shown in Fig. 1. Different gases were fully mixed in the blending device, and the mixed gas was introduced through the bottom of the furnace to participate in the reduction process. A computer program monitored the reaction temperature, the flow of various gases, and the weight of the sinters and recorded the weight data every 0.5 s. After the reduction process, the sinters were ground and analyzed by X-ray diffraction (XRD). The reduction process was divided according to the weight loss of the sinters. After reduction, the sinters were polished and characterized by scanning electron microscopy in conjunction with energy-dispersive X-ray spectroscopy (EDS).

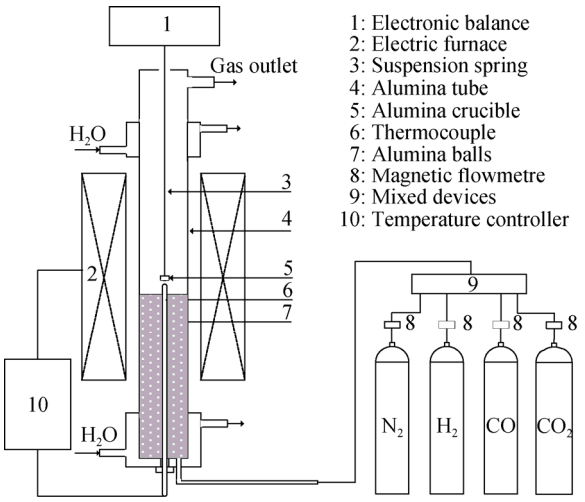

Fig. 1. Schematic of the reduction setup.

The reduction process of the sinters was also analyzed based on the calculation of Eqs. (1) and (2), shown as below, establishing the reduction kinetics models:

$$\mathrm{RI} = (0.11\times W_1)/(0.43\times W_2) + (M_0 - M_t)/(M_0 - 0.43\times W_t) \quad (1)$$

$$\mathrm{RI}' = \mathrm{dRI}/\mathrm{d}t \quad (2)$$

where RI is the reduction index of sinters; RI′ is the reduction rate of sinters, s^{-1}; M_0 is the initial mass of sinters, g; t is the reduction time, s; M_t is mass of sinters when the reduction time is t, g; W_1 is the FeO content in the sinters; and W_2 is the total content of Fe in the sinters.

3. Results and discussion

3.1. Analysis of the sinter reduction process

The isothermal reduction experiments of vanadium–titanium sinters were carried out at 800, 900, 1000, and 1100°C; the experimental results are shown in Figs. 2(a)–2(e). Fig. 2(f) shows the reduction conversion corresponding to different working conditions at 1000°C. As shown in Figs. 2(a)–2(e), the RI of the sinters increases gradually with increasing reduction time. The increase of the reduction temperature promotes RI in a rapid manner under different working conditions. According to the law of Arrhenius, the reduction rate increases exponentially with increasing reduction temperature. The higher the reaction activation energy, the more obvious the influence of temperature on the reaction rate. During the sintering reduction process by CO and H_2, the constant rate of the interfacial chemical reaction increases with increasing temperature, whereas the reduction rate increases as the other conditions remain unchanged. Under internal diffusion control, the diffusion coefficient is proportional to 1.57 times the change in temperature. In addition, with increasing temperature, the diffusion coefficient increases and the diffusion resistance decreases for CO and H_2 in the product layer [20].

Fig. 2(f) reveals that the RI values of different reducing atmospheres differed obviously. The main reducing agent of C1 was CO; however, the concentration of CO was low, resulting in a small increase of RI. The content of H_2 in the reducing gas increased after pulverized coal injection. As known from the thermodynamics analysis, the reducing ability of CO is stronger than that of H_2 when the temperature is less than 810°C; however, the opposite is true when the temperature is greater than 810°C. Meanwhile, the water–gas displacement reaction occurs, which would accelerate the reduction process of iron oxide due to the existence of H_2, contributing to the reduction effect of CO. In addition, in terms of kinetics, H_2 has an advantage over CO in the reduction process. The molecular dimension of H_2 is smaller than that of CO, and the diffusion velocities of H_2 and H_2O are higher in the production layer than those of CO and CO_2. During the reduction process, H_2 diffuses into the reaction layer earlier than CO and the reaction product H_2O diffuses from the reaction layer into the main gas earlier than CO_2. Therefore, from a diffusion aspect, the reducing ability of H_2 toward iron oxide is higher than that of CO. The RI is 0.478 for the sinters in C1, whereas the RI in the case of C4 is 0.758.

To quantitatively analyze the reduction characteristic of sinters under different conditions, we introduce the medium reduction index (MRE), which is defined as

$$\mathrm{MRE} = 0.5/t_{0.5} \quad (3)$$

where $t_{0.5}$ represents the time (in seconds) when the RI of the sinters is 0.5.

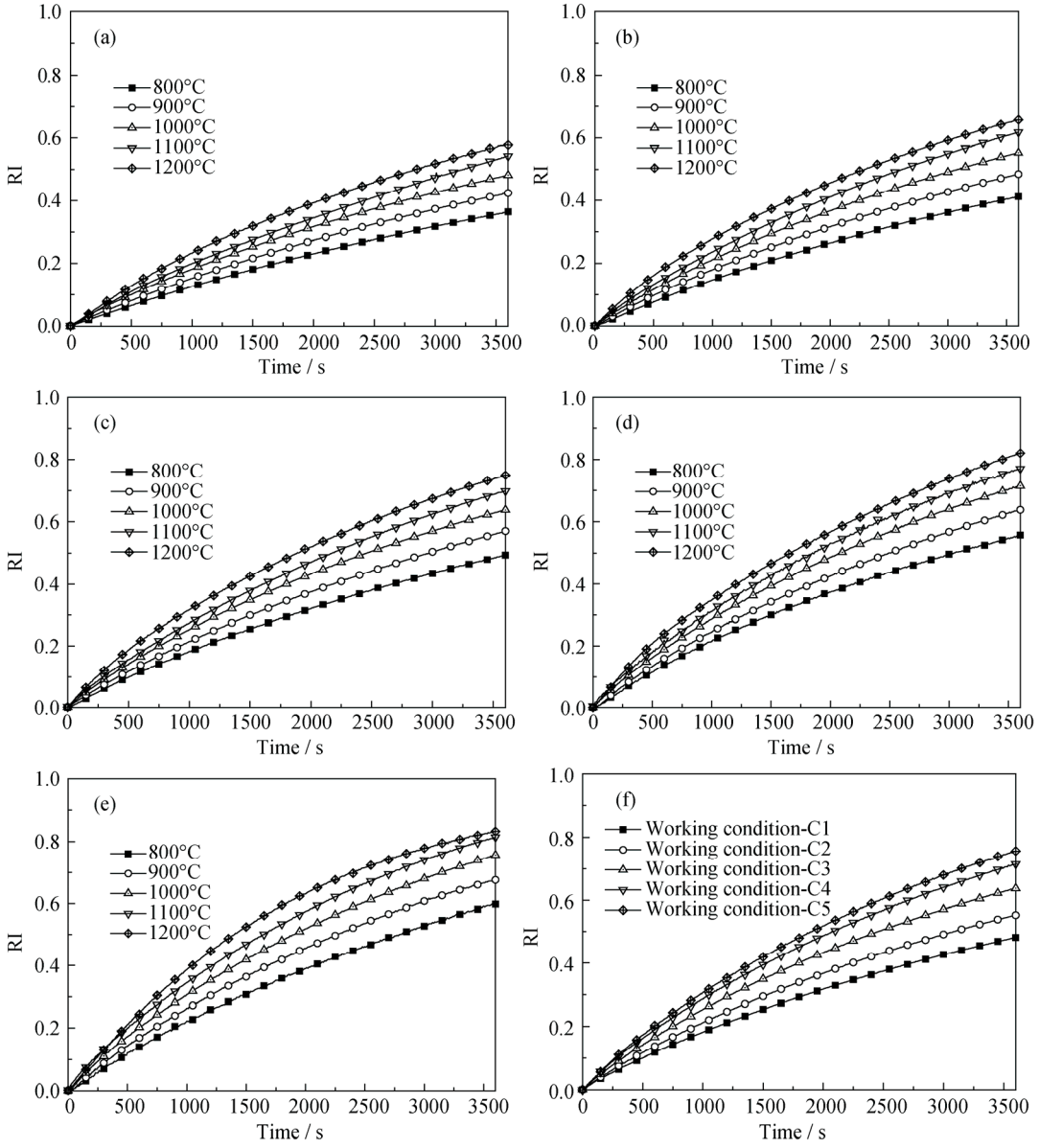

Fig. 2. RI curves of the sinters under working conditions C1–C5 at different temperatures (a)–(e) and RI curves under five working conditions at 1000°C (f).

Table 3 shows the MRE values under different working conditions for the sinters. The MRE value increases gradually with the increase of reduction temperature and the MRE value increases from 1.39×10^{-4} to 2.68×10^{-4} s^{-1} for C3 when the reduction temperature is increased from 800 to 1200°C. At the same time, the increase of CO and H_2 contents in the reducing atmosphere would improve the reduction properties. When the reduction temperature is 1000°C, the MRE value increases from 1.63×10^{-4} s^{-1} in the case of C2 to 2.66×10^{-4} s^{-1} in the case of C5. In addition, the change of the reduction properties between various oxygen enrichment pulverized coal injections and the reducing atmosphere was also investigated. Fig. 3 shows the relationship between the MRE value corresponding to oxygen enrichment under different working conditions. The MRE value increases and the range of MRE decreases gradually with increasing oxygen enrichment. The reason is that the increase in CO and H_2 contents has a decreasing characteristic in the reduction process.

Table 3. MRE values of sinters under different working conditions

Operating condition	MRE×10^4 / s^{-1}				
	800°C	900°C	1000°C	1100°C	1200°C
C1	—	—	—	1.75	1.55
C2	—	—	1.63	1.91	2.16
C3	1.39	1.71	2.05	2.33	2.68
C4	1.63	2.00	2.43	2.69	2.99
C5	1.79	2.19	2.66	3.02	3.60

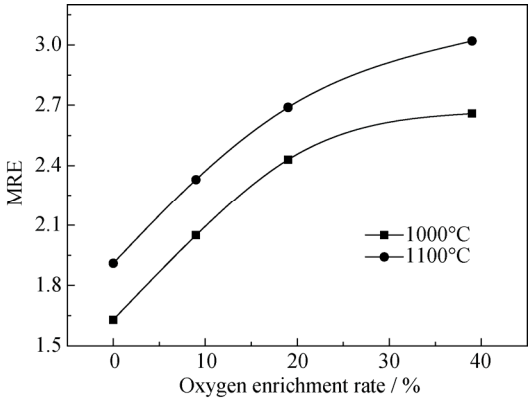

Fig. 3. Relationship between the MRE value and the oxygen enrichment potential.

3.2. Phase evolution analysis during the reduction process

The change of the phase evolution of sinters was also investigated. The divided samples were treated under the following conditions: (1) the working condition of C3; (2) a reduction temperature of 1000°C; and (3) a reduction time of 5, 10, 20, 40, or 60 min. After reduction, the samples were protected under an N_2 atmosphere until they had cooled to room temperature. A portion of each sample was ground for XRD analysis, and a portion was polished for SEM observation.

Fig. 4 shows the SEM results for the samples subjected to reduction for different times. The surface of the sinters was

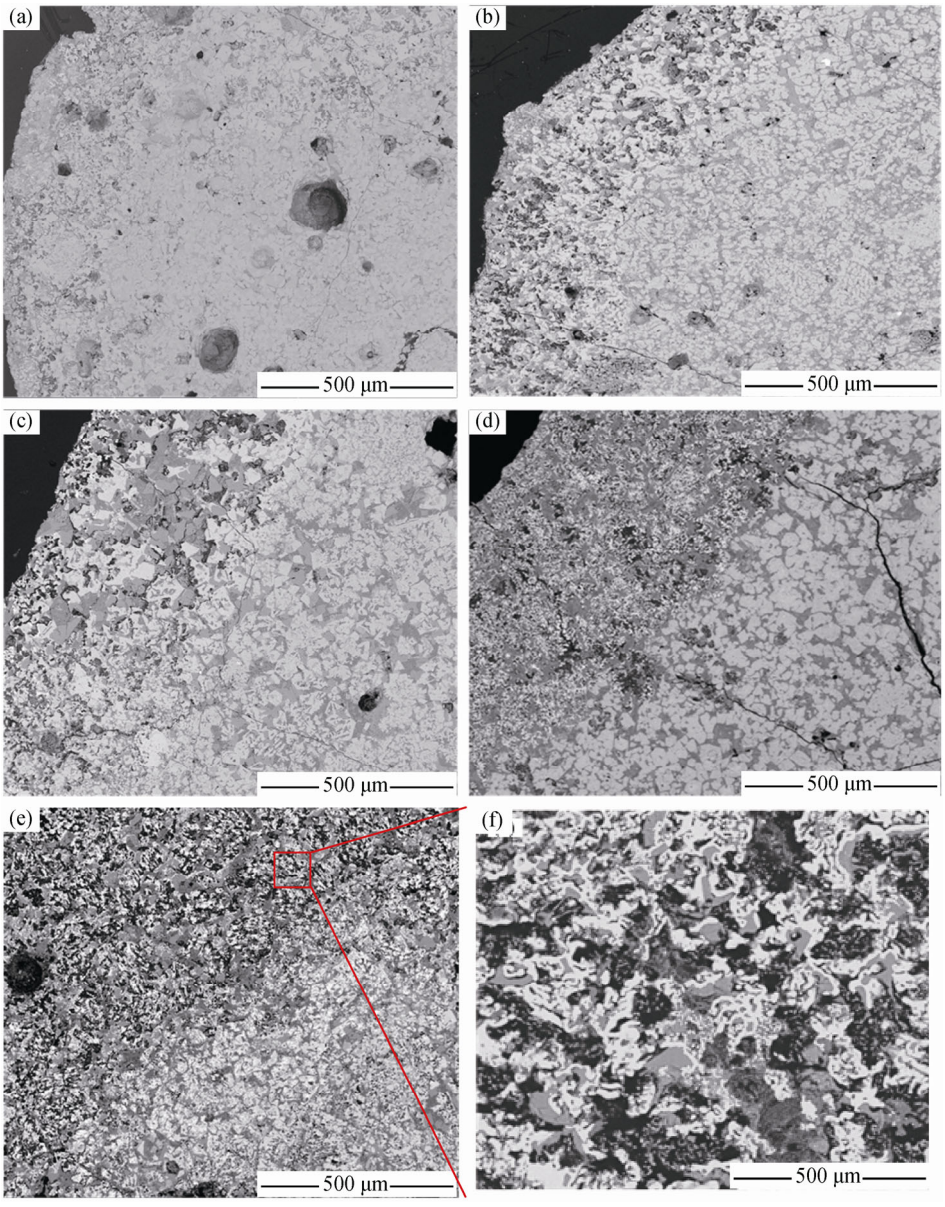

Fig. 4. SEM micrographs of the sinters subjected to 1000°C and the C3 working condition for various reduction times: (a) 5 min; (b) 10 min; (c) 20 min; (d) 40 min; (e) 60 min; (f) zoomed image of the area denoted with a red square in Fig. 4(e).

reduced to some extent; however, the inner part of the sinters was unreacted when the reduction time was 5 min. As shown in Figs. 4(a)–4(f), based on the analysis of the microstructure, the reduced zone increased with increasing reduction time and the reduced interface moved into the inner part. When the reduction time was 20 min, the ferrous phase was formed in the surface of the sinters while there was not any of that in the inner part, but it could be seen that there exited wustite. When the reduction time was 60 min, metallic iron was formed at the boundary of the sinters, and the reaction interface shifted to the center of the sinters. As shown in Fig. 4(f), most of the inner particles of the sinters were reduced to metallic iron, whereas a few unreduced iron oxides were surrounded by the dense iron product layer; small particles of iron oxide were observed as "unreacted cores."

For the further analysis of the sinters' microstructure after 60 min of reduction, Fig. 5 shows more detailed SEM images; the EDS analysis results corresponding to points 1–6 in Fig. 5 are shown in Table 4. The goal of these analyses was to deduce the relationship between titanium and ferrous ions in vanadium–titanium sinters during the reduction process. According to the results shown in Table 4, point 1 is wustite, which is still in the process of reduction; points 2–4 are the slag formed after reduction, where points 3 and 4 are the slag mainly composed by titanium. The interface between point 3, which is slag with titanium, and point 1, which is wustite, becomes much clearer with increasing the reduction time; by contrast, point 4 contains titanium combined strongly with wustite. Hence, point 3

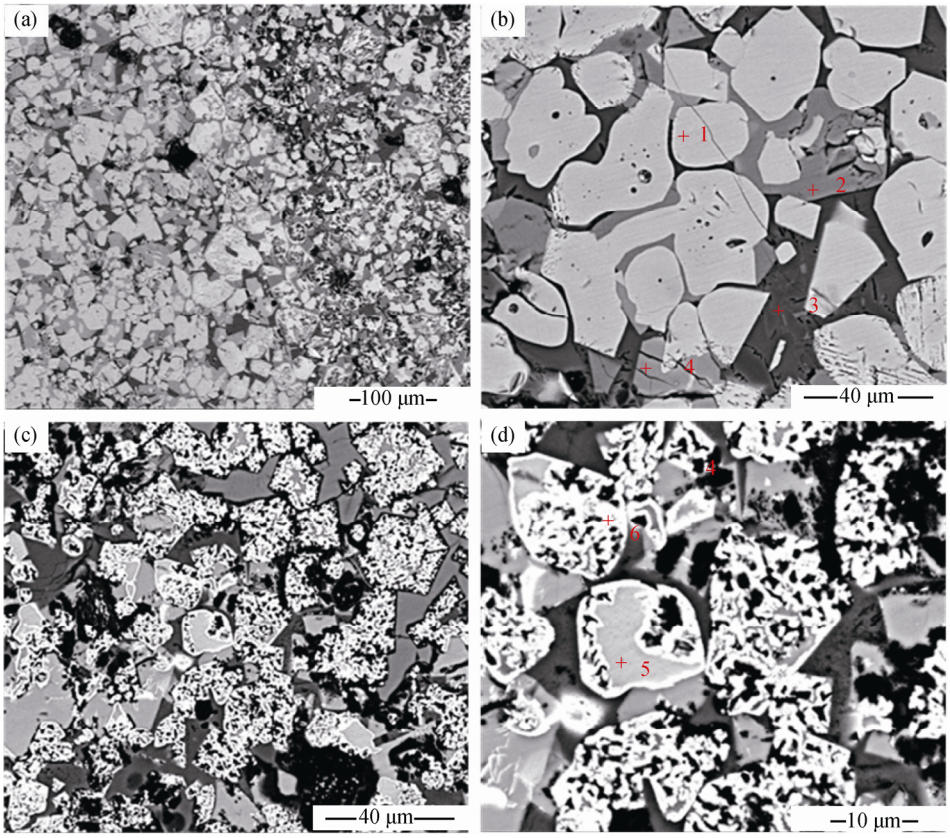

Fig. 5. Microstructure of the sinters after reduction (1000°C, C3, 60 min).

Table 4. Elemental compositions after reduction of sinters correspond to points in Fig. 5 wt%

Point	C	O	Mg	Al	Ca	Si	Ti	Fe
1	—	23.00	0.73	1.27	2.01	0.21	3.43	69.35
2	—	26.40	—	—	35.63	22.95	3.17	11.85
3	—	28.81	1.23	15.74	4.87	12.45	32.86	4.04
4	—	22.62	0.46	0.78	34.49	1.83	28.79	11.03
5	—	18.46	2.54	4.39	—	0.25	1.80	72.56
6	—	2.05	0.35	0.55	1.15	0.61	0.69	94.60

is reduced from point 4 to finally realize the reduction process of vanadium–titanium sinters. The EDS analysis results show that point 5 is wustite with small amount of titanium and point 6 is metallic iron with little titanium. We concluded that the reductive separation of titanium and ferrous ions during the reduction process is the critical controlling step influencing the separation between the iron and the slag.

Fig. 6 shows the XRD patterns of the sinter samples reduced for different times. The main minerals of the unreacted sinters are hematite, magnetite, and ilmenite. When the reduction time was 5 min, the peak of wustite appeared and the intensity of the hematite peak decreased; however, the intensity of the magnetite peak increased. When the reduction time was 20 min, the peak associated with metallic iron appeared and the intensity of the hematite peak continued to decrease, whereas the intensities of magnetite and wustite peaks increased and the ilmenite peak emerged. When the reduction time was 40 min, the intensity of the ilmenite peak disappeared and the peak of metallic iron was the most intense peak in the spectrum; in addition, the intensity of the wustite peak continually increased. According to the aforementioned analysis, the reduction process of sinters can be expressed as $Fe_2O_3 \rightarrow Fe_3O_4 \rightarrow FeO \rightarrow Fe$. The reduction from hematite to magnetite was relatively fast. The hematite was reduced completely to magnetite when the reduction time was 20 min. In addition, the magnetite was completed reduced to wustite when the reduction time was 40 min.

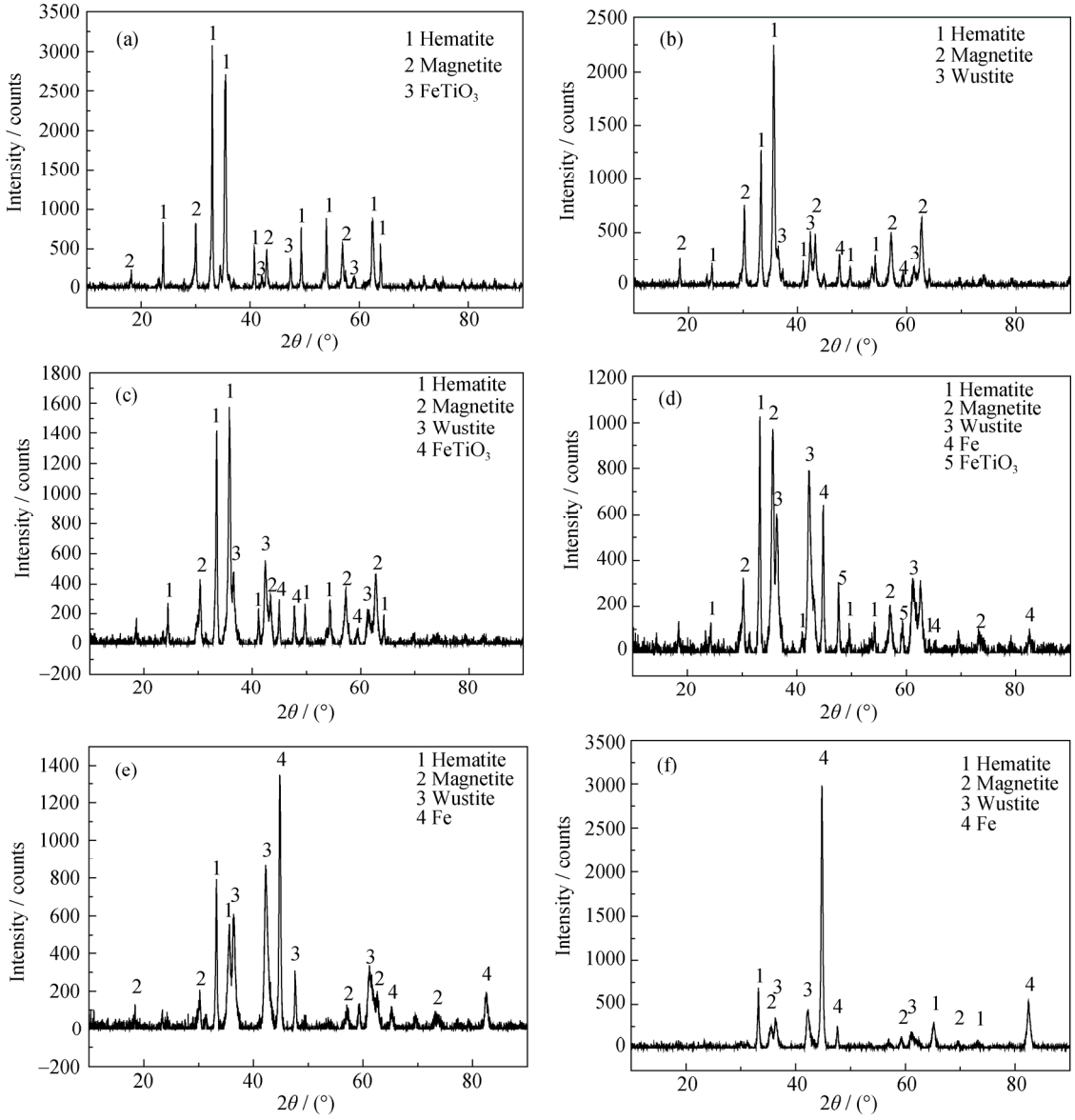

Fig. 6. XRD results of the sinters reduced for different times (1000°C, C3): (a) unreduced sinters; (b) 5 min; (c) 10 min; (d) 20 min; (e) 40 min; (f) 60 min.

3.3. Construction of the reduction kinetics model

For the gas–solid non-catalytic reaction, the reduction kinetic equation can be expressed as

$$\frac{\mathrm{d}\alpha}{\mathrm{d}t}=k\left(P_{\mathrm{g}},T\right)f\left(\alpha\right) \tag{4}$$

where α is the conversion rate (i.e., the RI); $\frac{\mathrm{d}\alpha}{\mathrm{d}t}$ is the reaction rate (i.e., RI′); k is the apparent reaction rate constant, whose value is influenced by the reaction temperature (T) and the gas-phase pressure (P_{g}); $f(a)$ is the function of the reaction kinetics mechanism; and t is the reaction time.

If the gas pressure is assumed to be constant during the reduction process, the apparent reaction rate constant is mainly influenced by the reaction temperature, which can be expressed by the Arrhenius formula:

$$k=k_0\mathrm{e}^{-E/RT} \tag{5}$$

where k_0 and E are the pre-exponential factor and the chemical reaction activation energy, respectively.

We applied three gas–solid reaction kinetic models to investigate the reduction of vanadium–titanium sinters in this research, including grain model (GM) [21–22], volume model (VM) [23–24], and hybrid model (HM) [25]. The mechanisms of different models vary; the reaction rates of the three models are expressed as

$$\mathrm{RI}'=k_{\mathrm{GM}}\mathrm{e}^{-E/RT}\left(1-\mathrm{RI}\right)^{2/3} \tag{6}$$

$$\mathrm{RI}'=k_{\mathrm{VM}}\mathrm{e}^{-E/RT}\left(1-\mathrm{RI}\right) \tag{7}$$

$$\mathrm{RI}'=k_{\mathrm{HM}}\mathrm{e}^{-E/RT}\left(1-\mathrm{RI}\right)^{n} \tag{8}$$

where k_{GM}, k_{VM}, and k_{HM} are the pre-exponential indices of the GM, VM, and HM gasification reactions, respectively; n represents the reaction order.

In previous studies, the modified random pore model (MRPM) [26] was proposed; its formula is

$$\mathrm{RI}'=k_{\mathrm{HM}}\mathrm{e}^{-E/RT}\left(1-\mathrm{RI}\right)^{n}\sqrt{1-\psi\ln\left(1-\mathrm{RI}\right)} \tag{9}$$

where ψ is a parameter of the particle structure, with the expression of $\psi=\frac{4\pi L_0\left(1-\varepsilon_0\right)}{S_0^2}$ (here, S_0, L_0 and ε_0 are the pore surface area, pore length, and solid porosity, respectively).

Eqs. (6)–(9) are four explicit formulae that describe the gasification fractional conversion RI′, the conversion rate RI, and temperature T. The kinetic parameters, including E, k_0, n, and ψ, can be calculated from experimental datasets using nonlinear least square fitting methods. The objective function can be written as

$$\mathrm{OF}=\sum_{i=1}^{N}\left(\mathrm{RI}'_{\mathrm{exp},i}-\mathrm{RI}'_{\mathrm{calc},i}\right)^2 \tag{10}$$

where $\mathrm{RI}'_{\mathrm{exp},i}$ is the experiment data; $\mathrm{RI}'_{\mathrm{calc},i}$ is the value calculated using a model; and N is the number of test values in experiments.

Fig. 7(a) shows the contrasting relations between the experimental data and values calculated using the four models. Obvious deviations were observed when the GM and VM were used to express the reduction process, whereas the HM and MRPM exhibited better agreement, especially the MRPM. A comparison of Eqs. (8) and (9) suggests that the MRPM provided better agreement because it was modified according to the HM. In addition, the MRPM considers multiple pore structures resulting from the structure of sinters. The reduction process of the sinters in this research was complicated. When CO was used to reduce the sinters, iron oxides were reduced in the sequence of $\mathrm{Fe_2O_3}\rightarrow\mathrm{Fe_3O_4}\rightarrow\mathrm{FeO}\rightarrow\mathrm{Fe}$, which resulted in three interfaces; the existence of $\mathrm{H_2}$ divided the reduction process into another three interfaces. For simplicity, the reduction process of the sinters under different working conditions was considered to result in six interfaces. The GM could only express one interface during the reduction, whereas the VM, which considered the reduction activity, considered diffusion into and from the particles simultaneously, which is not consistent with the phenomenon of obvious reaction zones and unreduced zones discussed in Section 3.2. The HM is an empirical formula, but it can only express the reaction mechanism process under multiple conditions; it cannot express the phenomenon of samples with multiple pore structures. Although the MRPM is an empirical formula, it combines the properties of both the RPM and the HM, and is therefore able to express the more complicated reaction mechanism. The lines in Fig. 7(a) represent the calculation curves by different models at various temperatures. From the calculation curves and experimental curves, the MRPM provides a better fit than the other investigated models. Figs. 7(b)–7(f) shows the contrasting relation of the experimental data and the values calculated using the MRPM. Good agreement was obtained between the calculated values and experimental data, demonstrating that the MRPM can express the reduction process of iron ores under different reducing atmospheres.

Table 5 shows the reduction kinetic parameters of the sinters under different working conditions obtained using the MRPM. The contents of CO and $\mathrm{H_2}$ in the reducing atmosphere increased with increasing oxygen enrichment. The reduction apparent activation energy of the sinters decreased gradually: the values for C1 and C5 were 23.2 and 20.4 kJ/mol, respectively. The decrease of the apparent activation energy promoted the reduction process of the sinters at the same reduction temperature and accelerated the reaction rate of the system. The results also show that the reduction kinetic parameter n decreased gradually with increasing oxygen enrichment: the

values for C1 and C5 were 1.27 and 0.89 kJ/mol, respectively. Compared with the calculated values of Ψ, the values were small for all of the investigated working conditions. The sinters contained numerous large pores but few small pores, which was the critical factor influencing the value of Ψ. However, for smaller values of Ψ, the MRPM and HM results became more similar, consistent with Eqs. (8) and (9). When the Ψ value was limited to zero, the results obtained using the MRPM and the HM were the same, which is the main reason why the calculated values were so similar for the two models.

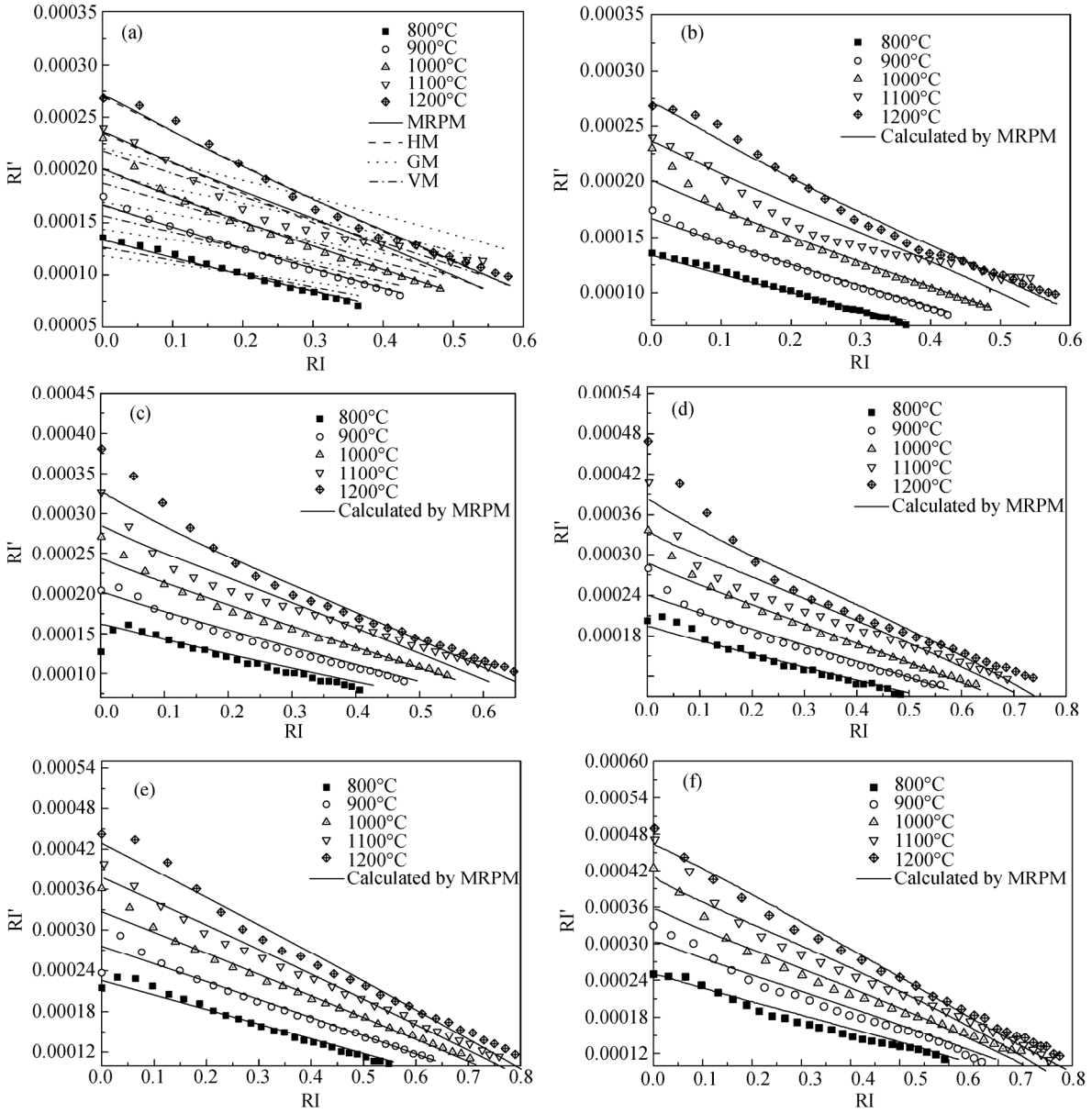

Fig. 7. Comparison of the calculated results of RI and RI′ and the experimental results of the sinters under different working conditions: (a) different models for C1, (b) C1, (c) C2, (d) C3, (e) C4, and (f) C5.

Table 5. Reduction kinetic parameters of sinters under different working conditions calculated by the MRPM

Working condition	k_0 / s^{-1}	E / (kJ·mol^{-1})	n	Ψ	R^2
C1	1.80×10^{-3}	23.2	1.27	9.12×10^{-6}	0.9729
C2	2.50×10^{-3}	23.0	1.20	1.29×10^{-7}	0.9696
C3	2.36×10^{-3}	22.3	1.04	6.52×10^{-7}	0.9565
C4	2.41×10^{-3}	21.1	0.93	1.24×10^{-6}	0.9361
C5	2.44×10^{-3}	20.4	0.89	3.17×10^{-8}	0.9691

4. Conclusions

In this research, the reduction behavior of sinters was investigated under different oxygen enrichment working conditions and the influence of reduction time and atmosphere on the reduction process was also analyzed, where the MRPM was used to investigate the reduction kinetic behavior under different working conditions. The results are summarized as follows:

(1) With increasing oxygen enrichment, the contents of CO and H_2 in the blast furnace coal gas increased, resulting in an increase in reduction rate of the reduction process of sinters. When the reduction temperature was 1000°C, the MRE value increased from 1.63×10^{-4} s^{-1} in the case of C2 to 2.66×10^{-4} s^{-1} in the case of C5.

(2) The MRE value increased from 1.39×10^{-4} to 2.68×10^{-4} s^{-1} under 9vol% oxygen enrichment when the reduction temperature was increased from 800 to 1200°C. However, the range of the MRE decreased gradually with increasing oxygen enrichment, indicating that the influence of the CO and H_2 contents in the coal gas on the reduction of sinters was diminished.

(3) Both the HM and the MRPM showed the changing relationship between the reduction rate and RI based on the analysis of the reduction process of sinters; however, the values calculated using the MRPM agreed better with the experimental data than those calculated using the HM. According to the calculation results of reduction kinetic parameters by the MRPM under different conditions, the reduction activation energy decreased to between 20.4 and 23.2 kJ/mol with increasing oxygen enrichment.

Acknowledgements

This work was financially supported by the Fundamental Research Funds for Central Universities (FRF-TP-15-063A1).

References

[1] X.P. Hu and M.Y. Liu, Application research on a high grade brazilian concentrates in sintering process, *Res. Iron Steel*, 38(2010), No. 2, p. 17.

[2] L.J. Yan, S.L. Wu, Y. You, Y.D. Pei, and L.H. Zhang, Assimilation of iron ores and ore matching method based on complementary assimilation, *J. Univ. Sci. Technol. Beijing*, 32(2010), No. 3, p. 298.

[3] J.G. Hu and Z.M. Gao, Characteristics of Marra Mamba iron ore fines and the application technology in sintering process, *Res. Iron Steel*, 36(2008), No. 5, p. 25.

[4] H.G. Li, G. An, Z.X. Zhao, and S.H. Ou, Experimental research on sintering performances of imported powder iron ores with high and medium ignition loss, *Met. Mine*, (2006), No. 8, p. 41.

[5] C.S. Deng, The reduction behavior and iron slag formation characteristics of vanadium–titanium sinter in blast furnace by dissecting 0.8 m^3 blast furnace, *Sichuan Metall.*, (1985), No. 2, p. 4.

[6] S.S. Liu, Y.F. Guo, G.Z. Qiu, T. Jiang, and F. Chen, Solid-state reduction kinetics and mechanism of pre-oxidized vanadium–titanium magnetite concentrate, *Trans. Nonferrous Met. Soc. China*, 24(2014), No. 10, p 3372.

[7] Y.Q. Bai, S.S. Cheng, H.B. Zhao, and S.F. Huo, Study of V–Ti sinter reduction degradation by mineralogical analysis, *Sintering Pelletizing*, 36(2011), No. 2, p. 1.

[8] Q. Lu, F.M. Li, W.S. Wang, and B.S. Hu, Influence of *w*(MgO) on sinter strength and sintering process of vanadium–titanium magnetite, *Res. Iron Steel*, 35(2007), No. 1, p. 5.

[9] M. Zhou, S.T. Yang, T. Jiang, and X.X. Xue, Influence of MgO in form of magnesite on properties and mineralogy of high chromium, vanadium, titanium magnetite sinters, *Ironmaking Steelmaking*, 42(2015), No. 3, p. 217.

[10] Z.G. Liu, M.S. Chu, H.T. Wang, W. Zhao, and X.X. Xue, Effect of MgO content in sinter on the softening-melting behavior of mixed burden made from chromium-bearing vanadium–titanium magnetite, *Int. J. Miner. Metall. Mater.*, 23(2016), No. 1, p. 25.

[11] G.Q. Yang, J.L. Zhang, J.G. Shao, Y.C. Wen, J.T. Rao, and W.G. Fu, Influence of vanadium titano-magnetite concentrate proportion on metallurgical properties of V-Ti bearing sinter, *Sintering Pelletizing*, 37(2012), No. 2, p. 6.

[12] Y.P. Sun, P.J. Liu, J.L. Lü, and J. Wang, Practice of blast furnace protection with titanium-containing sinter, *Iron Steel Vanadium Titanium*, 34(2013), No. 5, p. 48.

[13] J.J. Zhu and W.Z. Wang, Effects of PCI with oxygen enriched blast on the temperature field of the middle and upper zone in BF, *Iron Making*, 13(1994), No. 4, p. 19.

[14] A. Babich, S. Yaroshevskii, A. Formoso, A. Isidro, S. Ferreira, A. Cores, and L. Garcia, Increase of pulverized coal use efficiency in blast furnace, *ISIJ Int.*, 36(1996), No. 10, p. 1250.

[15] H. Ghanbari, F. Pettersson, and H. Saxén, Sustainable development of primary steelmaking under novel blast furnace operation and injection of different reducing agents, *Chem. Eng.*

Sci., 129(2015), p. 208.

[16] Y.S. Shen, B.Y. Guo, A.B. Yu, and P. Zulli, Model study of the effects of coal properties and blast conditions on pulverized coal combustion, *ISIJ Int.*, 49(2009), No. 6, p. 819.

[17] C.J. Yan, X.L. Cheng, J.J. Gao, and Y.S. Zhou, Effect of high oxygen enrichment PCI on BF blast ironmaking, *Iron Steel*, 48(2013), No. 6, p. 25.

[18] Z.Q. Hao, X.C. Li, and Q. Wang, Effect of metallization degree of burden on ironmaking operation of BF with oxygen enriched blast and coal injection, *J. Iron Steel Res.*, 12(2000), Suppl.1, p. 81.

[19] G.W. Wang, J.L. Zhang, J.G. Shao, H.B. Zuo, and J.Q. Qiu, Model for economic evaluation of iron production with oxygen-enriched and pulverized coal injection, *Iron Steel*, 48(2013), No. 11, p. 21.

[20] J.X. Li, P. Wang, and L.Y. Zhou, Technique of oxygen blast furnace with high injection of PC and hydrogenous fuel, *J. Iron Steel Res.*, 21(2009), No. 6, p. 13.

[21] J. Szekely and J.W. Evans, A structural model for gas–solid reactions with a moving boundary, *Chem. Eng. Sci.*, 25(1970), No. 6, p. 1091.

[22] J. Ochoa, M.C. Cassanello, P.R. Bonelli, and A.L. Cukierman, CO_2 gasification of Argentinean coal chars: a kinetic characterization, *Fuel Process. Technol.*, 74(2001), No. 3, p. 161.

[23] S. Kasaoka, Y. Sakata, and C. Tong, Kinetic evaluation of the reactivity of various coal chars for gasification with carbon dioxide in comparison with stream, *Int. Chem. Eng.*, 25(1985), No. 1, p. 160.

[24] J.Y. Shang and E.E. Wolf , Kinetic and FTIR studies of the sodium-catalyzed steam gasification of coal char, *Fuel*, 63(1984), No. 11, p. 1604.

[25] C. Shuai, Y.Y. Bin, S. Hu, J. Xiang, L.S. Sun, S. Su, K. Xu, and C.F. Xu, Kinetic models of coal char steam gasification and sensitivity analysis of the parameters, *J. Fuel Chem. Technol.*, 41(2013), No. 5, p. 558.

[26] J.L. Zhang, G.W. Wang, J.G. Shao, and H.B. Zuo, A modified random pore model for the kinetics of char gasification, *BioResources*, 9(2014), No. 2, p. 3497.